

Received 23 November 2022, accepted 30 December 2022, date of publication 4 January 2023, date of current version 17 January 2023.

Digital Object Identifier 10.1109/ACCESS.2023.3234185

RESEARCH ARTICLE

Dielectric Characterization and Statistical Analysis of Ex-Vivo Burnt Human Skin Samples for Microwave Sensor Development

PRAMOD K. B. RANGAIAH¹, (Member, IEEE), MOKHTAR KOUKI², YASMINA DHOUBI², FREDRIK HUSS^{3,4}, BAPPADITYA MANDAL¹, (Member, IEEE), BOBINS AUGUSTINE^{1,5}, MAURICIO DAVID PEREZ¹, (Member, IEEE), AND ROBIN AUGUSTINE¹, (Member, IEEE)

¹Ångström Laboratory, Division of Solid State Electronics, Microwaves in Medical Engineering Group, Department of Engineering Sciences, Uppsala University, 75121 Uppsala, Sweden

²Datamatrix AG, 2000 Neuchâtel, Switzerland

³Department of Surgical Sciences, Plastic Surgery, Uppsala University, 75105 Uppsala, Sweden

⁴Burn Center, Department of Plastic and Maxillofacial Surgery, Uppsala University Hospital, 75185 Uppsala, Sweden


⁵Uppsala Networked Objects (UNO), Ångström Laboratory, Division of Computer Systems, Department of Information Technology, Uppsala University, 75121 Uppsala, Sweden

Corresponding author: Robin Augustine (robin.augustine@angstrom.uu.se)

This work was supported in part by the Senseburn Project <http://www.senseburn.com/> through the Eureka Eurostar under Grant 2018/410, and in part by the Swedish SSF Project LifeSec under Grant RIT170020.

This work involved human subjects or animals in its research. The authors confirm that all human/animal subject research procedures and protocols are exempt from review board approval.

ABSTRACT The dielectric properties of skin tissues in relation to different degrees of burn are a necessary prerequisite for designing non-invasive microwave sensing modalities. Due to the difficulties in obtaining human tissue samples, such databases are largely unavailable. To bridge the knowledge gap in this field, we attempt to create a dielectric database of various burn-degree skin samples and their statistical analysis in this work. This research is part of the European “Senseburn” project, which aims to create a non-invasive diagnostic tool that can measure the severity and depth of burns on humans in a clinical setting. In this work, several ex-vivo burnt samples were collected from the Uppsala University Hospital (Akademiska sjukhuset, Sweden). Out of that, eight samples with different degrees of burns in various human body locations were selected for the analysis. The dielectric characterization of the categorized samples was done using a Keysight N1501A dielectric open-end co-axial probe Kit. The dielectric characterization was made from 500 MHz to 10 GHz with 1001 points. The measurement was made systematically, and the clinician feedback forms were gathered and analyzed throughout the process. The measurement data followed the FASTCLUS procedure, which was initially analyzed using density plot, convergence, and cubic clustering criteria. For the statistical analysis, 11 frequency points were considered for eight samples. The results of the fundamental statistical analysis using the FASTCLUS procedure resulted in 88 data sets. Later, data sets were analyzed in sample-wise clusters. Every sample was made with two clusters, i.e., cluster 1, which consisted of healthy sectors, and cluster 2, which consisted of burnt sectors. We made the linear approximations for the sample-wise clusters and found the constant real permittivity difference. Furthermore, we found a pattern in the constant real permittivity differences of every sample that is proportional to the burn degrees. This information is needed in order to identify optimization parameters, i.e., the sensitivity with respect to dielectric difference for various burn degrees. For this purpose, extensive measurement campaigns across the microwave frequency band from 500 MHz – 10 GHz were conducted. Based on the analysis of dielectric data, each skin region of interest (ROI) has its own dielectric properties. Additionally, we developed

The associate editor coordinating the review of this manuscript and approving it for publication was Md Asaduzzaman .

a proof of concept non-invasive flexible microwave sensor based on the dielectric database collected from burnt ex-vivo human tissue samples. In this way, we could distinguish between phantoms with different dielectric properties in the burned human tissue sample range.

• **INDEX TERMS** Burnt skin, permittivity, microwave profiling, statistical analysis.

I. INTRODUCTION

An appraised 180,000 demises annually are caused by burns, majority of this happened in low and middle-income nations [1]. Non-curable burn damages are a foremost cause of morbidity. Based on the analysis done by the American Burn Association (ABA), yearly over 450,000 severe burn injuries happen in the United States that necessitate medical treatment [2]. It is stated [2], “In 2014, around 3,275 verified deaths from fire and smoke inhalation injuries”. According to 2016 report from the Agency for Healthcare Research and Quality, the entire price for the handling of burns in 2010 was \$1.5 billion, with another \$5 billion in expenses related to lost work. So, ABA nominated a week between 2nd February 2020 and 8th February 2020 as National Burn Awareness Week. According to report [3], severe adult burns cases in Australia (Victoria) from 2007–2016 were identified using the Victorian State Trauma Registry (VSTR) and it calculated the economic burden to the state due to the injury. Excluding the year 2009, there were 7749 Disability-Adjusted Life Years (DALYs) which costed \$ 991,872,000. In Canada, more than 3200 people were admitted to Canadian hospitals for burns in 2005-2006 [4]. Between 1994 and 2003, over 10,000 children aged 0 to 19 years were admitted to a Canadian hospital with burn injuries. In Europe [5], out of studies conducted among 186,500 patients, almost 50% of patients were below 16 years, and almost 60% were male patients. The most prevalent causes of burn in the total population were flames, scalds, and contact burns. The groups with older patients, having higher total body surface area (TBSA), and groups with underlying chronic diseases had higher death risk. Sepsis after the injury and multi organ failure were the most frequently reported causes of death. Precise estimation of burn depth is important to decide the right treatment with dressings and surgery. The extent of burn injury may vary based on the living environment due to both intrinsic factors (provocative mediators, bacterial proliferation) and extrinsic factors (dehydration, systemic hypotension, cooling) [6]. That is why it is important to analyze the wound immediately to decide proper treatment by surgeons. A severe burn injury can lead to acute internal organ damages such as the kidney, due to activation of swelling and apoptosis, reduced renal perfusion, intra-abdominal hypertension, and acquaintance to nephrotoxic materials [7].

The percentage of TBSA is used to calculate the patient’s nutritional and fluid needs for the treatment. On the other hand, burn depth of the wound dictates the type of local and surgical treatment including skin grafting necessary to effectively reduce the damage. Burn wound depth is often difficult to determine by visual inspection of clinician and

distinguishing superficial partial thickness burns which does not need surgical intervention with deeper burns that needs grafting is challenging [8]. Relying of measurement tools allows more precise information to be collected. There are many state of the art non invasive techniques that enables to extract such information. These include Laser Doppler Imaging (LDI), Thermography, Videomicroscopy, Orthogonal polarization spectral imaging (OPSI), Reflectance confocal microscopy (RCM), Multispectral Imaging (MSI), Optical Coherence Tomography (OCT), Near Infrared Spectroscopy (NIRS), Terahertz imaging, Laser speckle imaging (LSI), Spatial frequency domain Imaging (SFDI), photoacoustic imaging and Ultrasound [9]. Among these, laser doppler imaging (LDI) has been shown to be reliable while others such as infrared thermography or spectrophotometric intracutaneous analysis have been less accurate [10]. However, these systems demonstrate few disadvantages when compared with permittivity-based microwave analysis in terms of cost, critical post-burn assessment time, and providing minimum discomfort to the patient. Except for ultrasound and photoacoustic imaging, most of these systems face limitations such as high cost, non-tolerance to the movement of the patient, non-conformity to the curvature of the measurement area, long scanning times, non-tolerance to ambient heat disturbances, etc. Our conformal sensors have the potential to mitigate these issues effectively and at a lower cost; however, the system needs standardization protocols for effectively quantifying burn depth. Thus, our present work in generating a dielectric database of different burn samples and its analysis is extremely important and helpful for establishing the standardization necessary to carry out noninvasive and effective burn depth analysis. FieldFox is used as Vector Network Analyzers (VNA) to measure reflection co-efficient measurements. The FieldFox was connected to the laptop consisting of IO (Input/Output) Libraries Suite 2020 and Materials Measurement Software. IO Libraries Suite 2020 [11] software inevitably senses FieldFox and configures the interfaces. Also, it allowed the material measurement software to measure the permittivity properties of the materials.

Burn damages are well-defined based on the depth of the wound, the modern classification technique of the burn degrees are, superficial, deep partial, deep dermal, and full-thickness [12]. Superficial burns comprise the most superficial layer of skin (the epidermis) only. These burns are not severe and successful healing is possible, can be treated by skin care products. Even though clinicians willingly treat superficial burns, the existing challenge is categorizing partial-thickness, deep dermal, and full-thickness burns.

Deep partial-thickness burns damage the entire skin layer (epidermis and dermis) and naturally need debridement and skin grafting. Full-thickness burns will damage the entire skin and reach down to hypodermis (adipose layer) needed debridement, skin grafting, and reconstruction [13]. Consequently, it is significant to distinguish the severity, burn degree, and depth to determine the proper treatment. The assessment of the degree and depth of the burn is done by a clinical evaluation. The accuracy of the clinical evaluation is estimated to be up to 70% [14]. There is also a very large variability between different assessors. In this work, we have considered the feedback of the burn specialist who operated on the patient. Also, we made clinician feedback forms and took the advice of many surgeons. Consistent diagnostic data is crucial for preliminary and effective medical interventions. A keystone in burn care is to evaluate the distribution and depth of the burn. The first parameter accounts for the affected area (size) of the body, the second for the affected tissues (depth). These two parameters determine the severity of the injury and, hence, the level of care and, also, constitute an “outcome” prognosticator, i.e. expected functional level after treatment [15], [16].

A. DIELECTRIC PROFILING BACKGROUND

This subsection provides the theoretical foundation required to comprehend dielectric characteristics and their measurement. Furthermore, a brief history of measuring the dielectric characteristics of biological tissues is presented to demonstrate how far dielectric measurements of biological tissues have progressed to this point. Human and animal tissues' dielectric characteristics have been studied by scientists in a variety of frequency ranges and with a variety of methods since the late 1940s [17], [18], [19]. The dielectric relaxation methods of biological materials would be further investigated and modeled in the 1980s [20], and the open-ended coaxial line became the most commonly used sensor for acquiring the dielectric properties of animal and human tissues [21]. Because it is non-destructive and can measure broadband signals both inside and outside the body, the open-ended coaxial measurement method was chosen over the transmission line, cavity perturbation, and tetra-polar probe methods [22]. During the same decade, several dielectric investigations were carried out, in addition to considerable developments being made in both the measurement method and the procedure. In addition to the dielectric characterization of human and animal tissues [23], the dielectric characteristics of the tissues were examined to see how they changed as a result of the physiological parameters of the tissues [24]. Dielectric properties in-vivo and ex-vivo were compared; the difference between healthy and cancerous tissues was investigated, and a report on the change in tissue dielectric properties after death was compiled. For example, the effect of tissue water content on dielectric properties at microwave frequencies was investigated [25], and dielectric properties in-vivo and ex-vivo were compared [26].

In conclusion, tremendous progress has been done over the previous three decades with the aim of enhancing existing dielectric measurement equipment. Both the enhancement of dielectric measurement equipment and the modification of the measurement technique contributed to these developments. In spite of this, additional dielectric data is still necessary to adequately cover all tissue types, temperature ranges, and frequency bands currently in use. This information will serve as the basis for future study on the impact of electromagnetic fields on burn degree analysis and the creation and improvement of new medical microwave sensors.

In our previous work, Perez et al [27] demonstrated substantial variability in the real permittivity in different human ex-vivo burnt samples based on the idea proposed by Papp et al [28] on the in-vivo animal tissue model. Later, we have described dielectric and color profiling of ex-vivo human burnt skin [29]. The key impression of the proposed work is based on different dielectric properties of skin in different burn conditions. Differences in dielectric properties have close relation with the hydration of the skin (as well as hypodermis). Consequently, determining the dielectric properties shows the confined hydration reduction caused by burn injuries. In clinical trials, the “clinical implication” of an outcome is reliant on its consequences on prevailing practice-treatment result size being one of the most significant aspects that drive treatment decisions. In our previous work, we have prepared the phantoms of the different burn degree samples and designed the microwave sensor to assess the burn depth [15].

We have used an open-ended coaxial probe technique for dielectric profiling. The open-ended coaxial probe consists of a truncated section of a transmission line [30], [31]. The electromagnetic field propagates along the coaxial cable, and reflection occurs when the electromagnetic field encounters an impedance mismatch between the probe and the tissue sample. When determining which probe to employ, it is important to take into consideration several factors, including sample size and heterogeneity, as well as the quality of the tissue surface. Surface imperfections have the potential to lead to poor probe-tissue contact as well as reduced repeatability in dielectric measurements. The open-ended coaxial probe is made from a shorter piece of a transmission cable. The electromagnetic field propagates along the coaxial line, and when it reaches the interface probe-tissue, due to the difference in impedance, the wave is reflected back. At different frequencies, the reflected signals are measured, and the results are used to figure out the complex permittivity of the material [29].

Statistical analysis significance depends on the sample collections, even minor treatment effects (which are clinically trivial) will demand good statistical analysis. Based on our previous experience in clustering the real permittivity values of the ex-vivo samples, we are using the FASTCLUS procedure. The FASTCLUS procedure computes distances from one or more quantitative variables to perform a disjoint cluster analysis [32]. The observations are divided into clusters

so that each observation belongs to only one. Because the FASTCLUS procedure uses Euclidean distances by default, the cluster centers are estimated using least squares [33]. This type of clustering method is commonly referred to as a “k-means” model. The least-squares criterion gets smaller with each iteration until convergence is reached because the cluster centers are the average of the observations given to each cluster when the algorithm is run to achieve convergence [34]. The FASTCLUS procedure is designed to work with large data sets containing 100 or more observations. The order of the observations in a small data set can significantly impact the results. Since the measured data are having a large number of data points, it is very important to choose the appropriate statistical analysis for the best way of data segmentation. Here we would like to explain the results based on the sample-wise clustering of healthy sectors and burnt sectors.

The remaining portions of the paper are structured as follows: Section II elucidates the experimental campaign, illustrating the experimental setup, visualization of the microwave dielectric property, and statistical analysis procedure. Section III provides results and discussion based on the statistical analysis with uncertainty and the targeted application. This work comes to a close with the discussion in Section IV.

II. EXPERIMENTAL CAMPAIGN

A. METHODS

The ethical approval was sort from the Swedish National Ethical Committee under the framework of the EUREKA Eurostars SenseBurn project on non-invasive Burn depth assessment. Permission for the study was granted by the Regional Ethical Review Board in Uppsala (Dnr 2018/410), tracked by biobank and hospital approvals on February 1st, 2019). Participating patients were supplied with information about the study and gave written informed consent for participation. If a participant was deemed incapable of providing consent at the time of initiation, written consent was first obtained from the patient’s next of kin and later from the participant. ICH-GCP (International Conference on Harmonisation – Good Clinical Practice) and the Helsinki declaration, and its subsequent revisions were followed. To avoid tissue drying, the time between excision and ex-vivo measurements is minimized. In addition to preventing differences in the tissue’s water content, efforts have been made to prevent temperature fluctuations in the sample. Tissues are carried in hermetically sealed containers due to the consistent effect of temperature on the measured dielectric profile.

All samples of burned human skin from surgical waste conforming to various burn depths, from full-thickness to superficial burns were collected from University Hospital’s Burn centre (Uppsala, Sweden) and the research was performed under relevant national ethical guidelines and regulations. The samples are not limited to any specific area of the human body, the metadata is maintained by the University Hospital’s Burn centre. Later, samples were brought to the

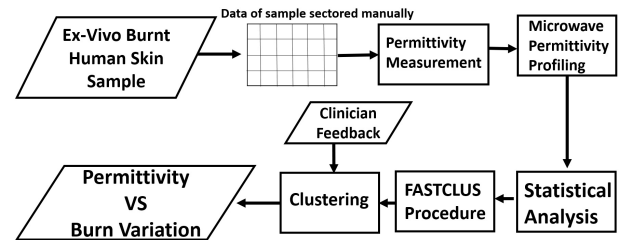


FIGURE 1. Outline of the technique for burnt variation and real permittivity analysis.

microwave lab (Ångström, Laboratory, Uppsala University, Sweden). The measurement form was maintained with clinical assessment of all the samples (S1-S8). Figure 1 shows a flowchart of the proposed technique, an overview of the process for microwave real permittivity characterization of the ex-vivo burnt human skin samples.

The process begins with the collection of the samples from the hospital. The ex-vivo burnt human skin samples were sectored manually, either sequentially or randomly, depending on the shape, burn variation, and size of the sample. The real permittivity measurement was performed based on the setup as described in the experimental setup section. The burned skin samples were not homogeneous, and the sectoring of the samples played a greater role in analyzing the burn variations in the samples. The measured values were examined statistically and discussed in a separate subsection. Every sample was plotted based on the sectors with corresponding real permittivity values to generate the microwave real permittivity profiling of the burn injury. Followed by the profiling, factual investigation was done using the FASTCLUS procedure to compute disjoint clusters of burnt variations in every sample. The clustering was done based on the clinician’s feedback. The real permittivity differences with respect to burned variations were obtained from the clustering.

In this work, eight ex-vivo samples are reported for the analysis. In normal clinical settings, it is not always possible to conduct measurements without significant delay, which may cause the tissue to dry out. Also, refrigerating for a longer time might introduce additional condensation, which might affect the measurement. In our case, clear protocols were established with our clinical partners to coordinate the excision date and time and transport the sample within a few hours for ex-vivo measurement. Figure 2 and Figure 3 shows the pictures of the samples. The table 1 shows the time records of the samples which include time of surgery (ToS), sample reception time (RxT) from the hospital, sample refrigerated time (ReT), and time of measurements (MeT). The thickness of the samples is measured by using a vernier caliper. Every sample raw image and manual clustered image are displayed one below another. When the surface of the tissue is characterized, it is possible to determine which areas of the tissue or specific points within the tissue are best suited for the acquisition of dielectric information. For example, thick samples with smooth surfaces are better than thin samples with rough surfaces so that the probe can get a

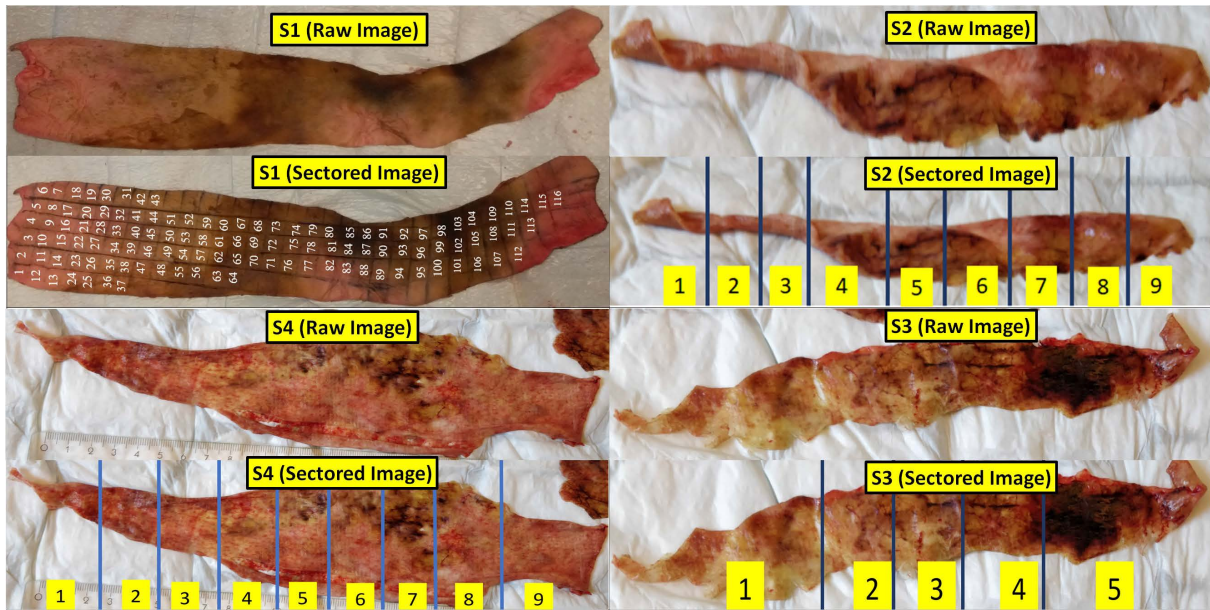


FIGURE 2. Raw and sectorized photographic images of S1 to S4.

TABLE 1. Time record of the samples which includes time of surgery (ToS), sample reception time (RxT) from the hospital, sample refrigerated time (ReT), and time of measurements (MeT).

Sample	Date	ToS	RxT	ReT	MeT
S1	3/3/2019	10:55	13:00	14:00 - 16:00	14:30 - 22:00
S2-S5	5/9/2019	15:10	15:56	Not Stored	16:30-19:30
S6	5/10/2019	11:15	12:38	13:00-13:45	14:20-15:10
S7, S8	6/5/2019	14:00	16:39	16:55-17:10	17:30-21:10

good grip on the tissue sample. When measuring on uneven tissue surfaces, our previous research [29] has shown that using smaller probes manufactured by Keysight Technologies yields more accurate results. This is especially true when the area being measured is limited or spatially restricted. Sample 1 (S1) shown in Figure 2 was received from the hospital and sectorized manually by 1 × 1 cm (total 116). The sample is from the lower extremity and abdomen. The sample was cut down to the fat layer. According to the clinical analysis, the sample was found to be deep dermal to full-thickness burn. The thickness of the sample was around 6.2 mm.

Sample 2 to 5 (S2 to S5) as shown in Figure 2 and Figure 3 was taken from the hospital and the sample thickness was around 1.2 mm (thin). The sample is sectorized manually and randomly based on the clinician’s inference and color identifications. Every sector was measured with the number of repetitions (three measurements at the center and random five measurements at various locations inside the sector). In total, 8 measurement values were taken in every sector. The sample is mostly from the narrow strips on the hands and the fingers. S2 and S3 were found to be full-thickness burns according to the clinical analysis. Again, S4 was found to be deep dermal burn and S5 was deep dermal to full-thickness burn.

Sample 6 (S6) as shown in Figure 3 consists of 5 small pieces and thickness was around 2.1 mm. The sample quality

was thin and soft. Every small piece was considered as sector and measured center 3 repetitions measurements and randomly 5 measurements are done. The clinician suggested the sample is of deep dermal burn and maybe full thickness in a few areas. The samples below are applied to the hands and fingers of the human body. S7 and S8 as shown in Figure 3 were having two medium-size pieces and the thickness is around 1.5 mm. The sample was sectorized randomly as shown in Figure 3. Every sector was measured with 8 values, 3 at the center of the sector and 5 randomly over the sector. According to clinical analysis, the sample was from lower extremity and partial-thickness to deep dermal injury. Every sample’s thickness and burn variations are tabulated in Table 4.

B. DIELECTRIC CHARACTERIZATION EXPERIMENTAL SETUP

The figure 4 shows the experimental setup used for the dielectric characterization of the ex-vivo burnt skin samples. The setup included Keysight N1501A Dielectric Probe Kit [35] and Combination Analyzer N9918A FieldFox Handheld Microwave Analyzer. The measured data from the FieldFox does not result in a convenient format. So, N1501A Dielectric Probe material measurement software E07.02.29 was required to convert data from FieldFox to permittivity values. The LAN cables were used to interface between the laptop and FieldFox. Good quality RF cables were used to connect dielectric slim with FieldFox for quality measurements. The power level of the FieldFox used -15 dBm and intermediate frequency (IF) bandwidth of 300 Hz for the best results.

The complex permittivity ($\epsilon(\omega)^*$) of biological tissues (as well as polar materials) is what determines their dielectric properties; this property defines how the tissue interacts with an electric field that is applied from the outside. A charge

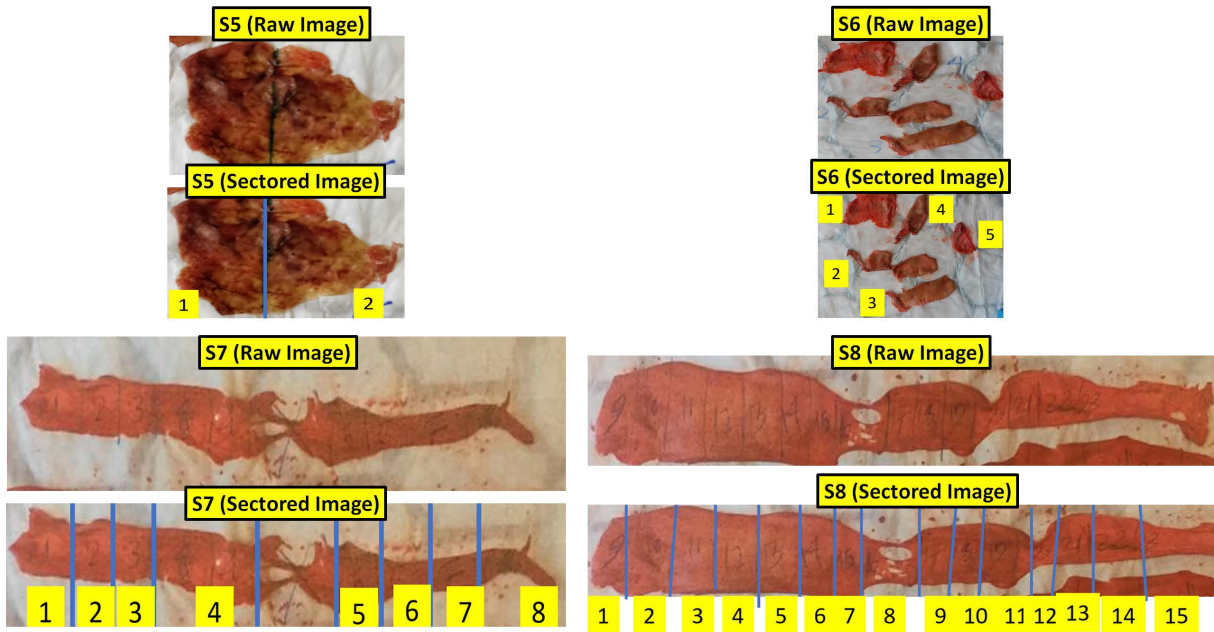


FIGURE 3. Raw and sectored photographic images of Samples 5 to 8.

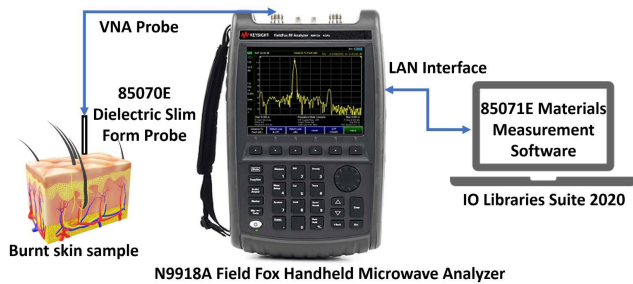


FIGURE 4. Dielectric characterization experimental setup.

displacement in the tissue that results from the application of an electric field is what produces dielectric polarization. The real and imaginary terms of the complex permittivity are connected to one another by the Equation 1:

$$\epsilon(\omega)^* = \epsilon'(\omega) - j\epsilon''(\omega) = \epsilon'(\omega) - j\frac{\sigma(\omega)}{\omega\epsilon_0} \quad (1)$$

where ω is the angular frequency, ϵ' is the real part of the complex permittivity (dielectric constant), the dissipative property of the tissue, which absorbs the energy and partially transforms it into heat, is reflected in the imaginary component of permittivity ϵ'' .

1) PROBE AND EX-VIVO TISSUE CONTACT

The open-ended coaxial slim probe tip is cleaned before placing on the ex-vivo tissue. The sufficient force is applied against the tissue without destructing. We make sure to have good contact between the probe and tissue. Therefore, no air bubbles or uneven sample surfaces are present to disturb the measurements. Typically, in ex-vivo scenarios,

the probe–tissue contact is verified by visual inspection; however, this approach is challenging in a surgical setting. According to the author’s experience, it is more convenient to move the sample towards the probe using a lift table until the entire probe aperture makes firm contact with the tissue sample, as opposed to moving the probe during the measurement procedure, in order to reduce the uncertainty caused by probe and cable movement in ex-vivo measurements.

In fact, using a constant pressure results in more accurate measurements. For each sector, we repeated the measurements numerous times [36]. There are currently very few studies in the literature that quantify measurement error in terms of applied pressure change. The researchers have carried out a number of experiments to quantify the inaccuracy caused by fluctuations in probe pressure, but they noticed that the results could not be generalized to all of the measurement locations within the sample. For instance, variations in sample thickness, tissue mechanical characteristics, water content, and surface imperfections may exist within the same tissue sample, necessitating the use of several probe pressures on the same sample. As a result, it is impossible to report a single, fixed pressure for all samples. However, the following method could be applied to get a good contact: To get the probe in touch with the sample, a little amount of pressure is first applied. If this low pressure is sufficiently low, further measurements conducted at the same location may produce inconsistent readings (due to air gaps). If this happens, the pressure can be adjusted until measurements taken at the same spot are repeatable. On the other hand, if applied with excessive force, high pressure can injure tissue by compressing the tissue and causing internal fluid to leak out onto the tissue surface [37], [38].

2) SURFACE SCATTERING

The method through which microwave radiation that has impacted a solid or liquid surface is either completely or partially redirected away from it. Ex-vivo tissue can be considered as a semi-solid substance. Surface scattering only arises at the point where ex-vivo tissue, a homogeneous material into which electromagnetic (EM) energy is incident, contacts the probe tip surface. Increases in complex permittivity cause an increase in microwave scattering on the ground, while surface roughness affects both the scattering direction and magnitude. If the surface is smooth, there will be a specular reflection at an angle that is symmetric to the incident angle. Fresnel reflectivity, which develops together with the ratio of complex permittivity, determines the strength of the specular reflection. Both a specular reflection and a scattering component are present as the surface roughness rises. While the scattering component is referred to as the diffuse or incoherent component, the specular reflection component is known as the coherent component. We considered the ex-vivo tissue to be a smooth surface, and the EM waves reflected from the ex-vivo tissue that we experimented with were very slightly out of phase with one another. If two points on the surface differ in height Δh , waves reflected from those points will have the relative phase difference $\Delta\phi$ shown in Equation 2

$$\Delta\phi = \frac{4\pi \Delta h \cos \theta_i}{\lambda} \quad (2)$$

If this phase shift is less than 90, which leads to the Rayleigh criterion, then it is plausible to expect a surface to be smooth (Equation 3). It is recommended that surfaces be considered smooth only if the roughness is less than one-quarter of the value indicated by the Rayleigh criterion (i.e., the phase difference is less than $\pi/8$). Surfaces of any roughness can be considered smooth for $\cos \theta_i = 90$ because all reflected rays arrive with the same phase shift.

$$\Delta h = \frac{\lambda}{8 \cos \theta_i} \quad (3)$$

3) TEMPERATURE CONSTRAINTS

Transporting tissue in hermetically sealed, temperature-controlled containers is typically required since the temperature consistently affects the measured dielectric spectrum of living tissues. In earlier research [39], the dielectric properties of biological tissues were measured at discrete frequencies and temperatures. For slight temperature variations, the results were expressed in terms of linear temperature coefficients, which are the percentage change in conductivity or permittivity per degree Celsius. We considered the water standards during the slim probe's calibration. The water standard has parameters for temperature, and it was consistently determined that the water within the lab was 21 to 22 degrees Celsius. The temperature of each ex-vivo tissue sample was noted; it should be between 23 and 25 degrees Celsius. Depending on the tissue and the frequency and temperature range under consideration, the change in relative permittivity in the microwave frequency range is, at most, 2% per degree

Celsius, and the change in conductivity is between 1% and 2% per degree Celsius [40], [41]. The relative permittivity and conductivity trends with temperature typically show different directions throughout time. However, in most biological tissues at lower frequencies, the magnitude of change in permittivity and conductivity per degree Celsius tends to be higher. In conclusion, the consideration of tissue type, frequency, and temperature range all affect the conductivity and permittivity temperature coefficients. We know these temperature coefficients and utilize them to account for temperature changes during tissue dielectric measurements.

Every measurement of the samples was made after calibration of the device with a slim probe calibration kit. FieldFox was started and prewarmed at least 15 minutes before the measurements. The user-defined calibration options like air, water, and short were utilized. The temperature parameters were taken into account in the data analysis part. The measurement of the complex permittivity of the burnt human skin samples was saved in the '.prn' format with the help of Materials Measurement Software. Also, the software helps us to conveniently save the data as permittivity versus frequency.

C. MICROWAVE PERMITTIVITY PROFILING

In this subsection, the microwave permittivity profiling of the samples based on the measured permittivity is explained. Figure 5 shows the microwave permittivity profiling of all samples. The image was prepared based on the physical dimensions of the sample. Also, the real permittivity values of every sector were the average of the measurement repetitions done in the corresponding sector. Later, the image was normalized with reference of L'Istituto di Fisica Applicata "Nello Carrara" (IFAC) data [42]. The IFAC in Florence developed a parametric model-based application for calculating the dielectric properties of tissues and organs. The skin, subcutaneous fat, and muscle data have been derived from the IFAC application, and the skin was assumed to be dry.

S1 consists of 116 sectors, every sector was having different real part permittivity values. The sample was discretized to 116 sectors and the measurement was done for five repetitions at different parts of each sector. Five iterations at different locations of each sector and the sector near the edge have a larger deviation due to the thickness. We tried to measure data from sectors that are far from the boundary. Finally, the mean values of each cell are reported. Since the sector was made sequentially 1 cm \times 1 cm. We have plotted the image as 6 rows and 32 columns. The real permittivity values were normalized with IFAC data, for example, dry skin values (at 2.45 GHz real permittivity as 38). The scale of the image was made accordingly to the real permittivity variation. We used a deep blue to signify low real permittivity and a bright yellow to denote nearly high real permittivity. The unmeasured area was colored the deepest blue without any numerical values being applied to it. In later sections of the article, the clustering results are explained statistically. S2 consists of 9 sectors, sectors were made random. So, real permittivity profiling was plotted with a single row

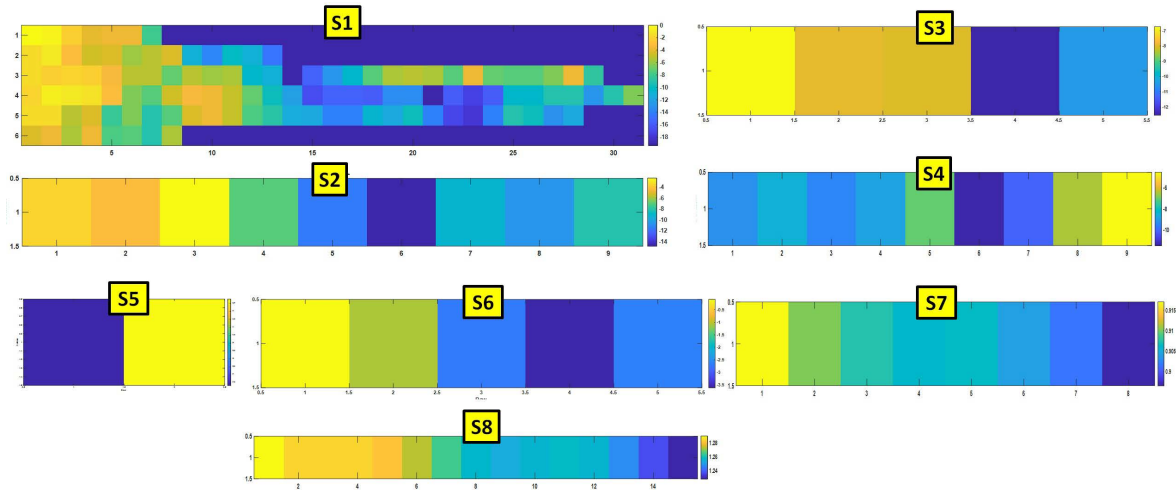


FIGURE 5. Microwave permittivity profiling based on the real part permittivity of all the samples.

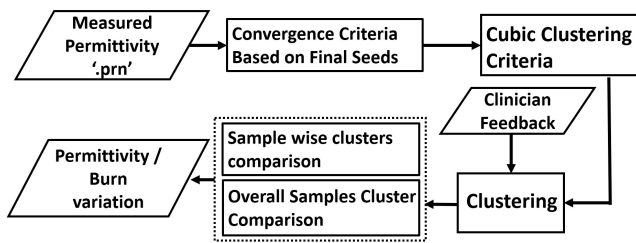


FIGURE 6. Flowchart of FASTCLUS procedure used for the burnt skin analysis.

and 9 columns. Every sector was having 8 measurements, an average of 3 measurements which was done at the center of the sector. With that average, the rest 5 measurements done randomly were considered statistically to assign the values to the imaging plot. The same procedure was followed for the rest of the samples. S3 is having 5 sectors, so imaging has a single row and 5 columns. Similarly, S4 got 9 columns, S5 got 2 columns, S6 got 5 columns, S7 and S8 got 8, 15 columns correspondingly.

D. THE FASTCLUS PROCEDURE

The FASTCLUS procedure was used in this work to perform a disjoint cluster analysis to investigate the real permittivity variations in burnt human skin ex-vivo samples. This technique was used in the segmentation of real permittivity values of the sectors of the samples. Initial work of the FASTCLUS procedure involved preparing the data for the clustering based on the burn variations which includes missing data handling, outliers [43], standardizing, and reduction of variables using the FACTOR procedure [44]. The Figure 6 shows the detailed flowchart of the FASTCLUS procedure used for the burnt skin analysis.

Some of the highlights of the FASTCLUS procedure features used are:

- The Euclidean distances used for the clustering centers are based on the Pseudo F statistic and observed overall R-squares estimation (k-means model).

- Based on clinician feedback, real permittivity microwave profiling, and data sets, the optimal method for locating good clusters is compelled.
- Cubic clustering criterion was used along with approximate expectation overall R^2 .
- Used for the effective technique for noticing outliers since it regularly appears as clusters with a solitary individual member.
- The proposed work makes use of large data sets of real permittivity measurements (more than 820 classified files) as well as additional annotations.
- The development of algorithms that have a greater impact on variables with greater variance.
- Calculated subjective cluster means and median, displayed summaries of the clusters.
- Produced an output data set containing cluster 1 (healthy) and cluster 2 (burnt) associated real permittivity and created a SAS dataset that resembles output tables 2 and 3.

III. RESULTS AND DISCUSSION

According to Figure 5, it is clear that the highlighted cells are less damaged and the dark cells are severely damaged, that is their permittivities are reduced drastically to fat real permittivity based on the clinician analysis. When we compared the measured values with the IFAC-CNR catalogue [45] the real permittivity of sectors was matching superficial dermal burns with typical dry skin values. Deep dermal and full-thickness real permittivity values of the sectors were similar to the values of bone and fat. When the microwave real permittivity profiling was done, we received a good correlation of the real permittivity values with burn degree variations. The power level of the FieldFox used -15 dBm and intermediate frequency (IF) bandwidth of 300 Hz for the best results. Every sample clustering is made based on clinician feedback. The clustering results will be displayed in two ways i.e., overall samples-based clusters and sample-wise clusters.

TABLE 2. Average of average real permittivity versus frequency of cluster 1 (Healthy and negligible burnt sectors).

Frequency (GHz)	AOA real permittivity of Cluster 1 (Healthy sectors)							
	S1	S2	S3	S4	S5	S6	S7	S8
1	35.9	37.7	21.5	13.8	20.1	45.1	46.4	48.7
1.5	34.8	36.2	20.5	13.4	19.3	43.9	45.0	47.3
2	33.6	35.4	19.9	6.2	19.1	42.9	38.8	46.2
4	29.9	32.0	17.3	11.9	17.1	39.3	41.2	36.9
4.5	29.2	31.5	17.1	11.7	16.8	38.7	35.4	40.9
4.8	28.7	31.0	16.6	10.8	15.6	38.3	40.0	35.8
5	28.6	30.9	16.6	11.2	16.2	38.0	39.8	35.1

TABLE 3. Average of average real permittivity versus frequency of cluster 2 (burnt sectors).

Frequency (GHz)	AOA real permittivity of Cluster 2 (Burnt sectors)							
	S1	S2	S3	S4	S5	S6	S7	S8
1	16.0	19.1	14.6	5.6	8.4	37.7	40.7	42.5
1.5	15.5	18.0	13.8	5.8	8.5	36.6	39.5	41.4
2	15.0	17.4	13.2	13.4	8.7	35.6	44.2	40.5
4	13.0	15.0	11.1	5.6	8.0	32.2	36.1	41.7
4.5	12.7	14.9	11.2	5.6	7.9	31.6	40.4	36.3
4.8	12.4	14.7	11.0	4.9	7.2	31.3	35.0	40.3
5	12.4	14.7	11.1	5.2	7.5	31.0	34.8	39.8

Table 2 shows the values of the average of average (AOA) real permittivity of cluster 1. Cluster 1 includes the real permittivity values of the healthy sectors or negligible burnt sectors of the samples. The sectors were determined healthy or burnt by the sample color variations and clinician feedback. We can observe the real permittivity values of every sample with respect to frequency. The average values of cluster 1 decrease linearly with respect to frequency. In every sample, there are multiple sectors which are explained previously in the ex-vivo section. Every sector has multiple measurements, smaller sectors have 3 measurements, and larger random sectors having 8 measurements. The average of all the sector-wise measurements was calculated, similar burnt variations sectors were made as clusters. In Tables 2 and 3, a consists of average of all the belonging sectors in the cluster is averaged again. So, values are called as AOA real permittivity of the clusters with respect to frequency points.

Table 3 shows the values of the AOA real permittivity of cluster 2. Cluster 2 includes the real permittivity values of the burnt sectors of the samples. The burnt sectors were identified by the clinical expert, and clusters were made accordingly.

A. SAMPLE-WISE CLUSTERING COMPARISON

To present the concept evidently, the findings are explained in this subsection. Figure 7 shows the sample-wise clustering comparison of S1 to S4. Every sample is explained based on the real permittivity variation between cluster 1 and cluster 2. In every plot, the curves are analyzed with a linear trend-line for the best fit of the curves. The linear curves are plotted by leveling the regular pattern, displayed with equation and R^2 values, to discuss the real permittivity variations between the clusters curves. All curves were found to be almost linear, every curve R^2 value were found to be greater than 0.9 (1 is ideal).

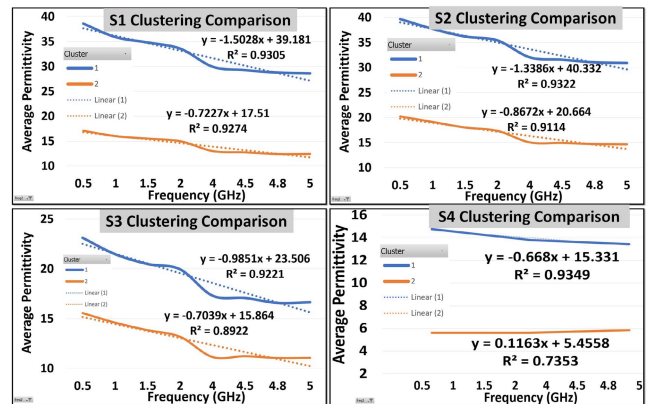


FIGURE 7. Sample-wise clustering comparison of samples 1 to 4.

S1 was found to be deep dermal to full-thickness burn based on the clinician’s feedback. The data is in congruence with the convergence criterion and is made into two clusters. Cluster 1 (Healthy) real permittivity variations are having higher values compared to Cluster 2 (burnt) real permittivity variations. Pseudo F Statistic [46] define the ratio between inter-cluster and intra-cluster variance. Pseudo F Statistic is found to be good value 1730.46, also observed over-all R^2 as 0.71 and approximate expected over-all R^2 was 0.75. Cubic clustering criterion was applied for the clustered data. The same steps are performed for the rest of the frequency points until 5 GHz. For S1, the separated cluster curves were found as shown in Figure 7. The frequency responses of the clustered data were found to be linear based on the trendline concepts, whose equations and R^2 are displayed in the Figures 7 and 8. This pair of linear equations can be solved using the Gaussian elimination method [47], [48], Cramer’s rule [49], Rouché–Capelli theorem [50], etc. The curves are found to be linear, but the slope of the equations is not the same (not parallel lines). So, an approximate difference between the two lines can be found by taking the difference of the values of the constants of the equation. S1 cluster curves difference is found to be 21.68. Similarly, every sample analyzed for the frequency between 500 MHz to 5 GHz and the corresponding results were plotted. Figure 8 shows the sample-wise clustering comparison of S5 to S8.

Some research groups claim that the Keysight N1501A dielectric open-end coaxial probe has a penetration depth greater than 1 mm, but Meaney et al. [51], recently demonstrated that the penetration depth of the slim probe is less than 1 mm. We also placed the tissue samples on the bed spread, which was a polyester and cotton blend (poly-cotton), while conducting the measurements. The bedspread is 1.1 mm thick, which prevents back reflection and disturbance of the electric field. The measurement table is completely anti-static, and the configuration is appropriate for characterization. Furthermore, we observed the air real permittivity by placing the slim probe just 1.2 mm above the water level in several experiments. However, research is being conducted to improve penetration depth by employing

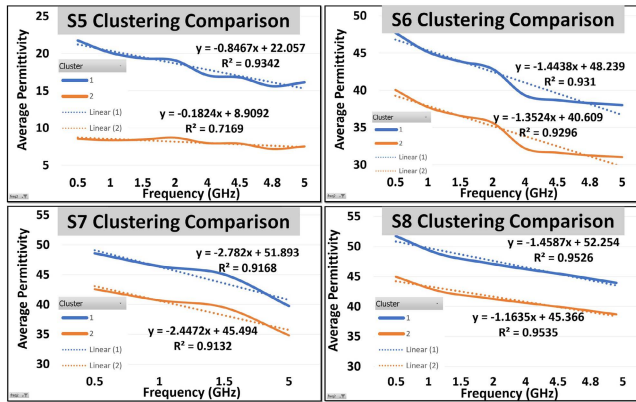


FIGURE 8. Sample-wise clustering comparison of samples 5 to 8.

TABLE 4. Relationship between the constant difference of the clustered curves and burn variations.

No	Thickness (mm)	real permittivity difference	Remarks
S1	6.2	21.68	Deep dermal to full thickness
S2	1.2	19.67	Full thickness
S3	1.2	7.64	Deep dermal
S4	1.2	9.93	Deep dermal
S5	1.2	13.14	Deep dermal to full thickness
S6	2.1	7.62	Deep dermal
S7	1.5	6.39	Partial-thickness to deep dermal
S8	1.5	6.88	Partial-thickness to deep dermal

two probes and a transmission method. As the penetration is small, the lateral confinement is also small. It is even more critical to press the probe well against the tissue to ensure good contact with the central pin and the probe’s border. Ideally, we try to get the probe immersed in liquids for at least 5 mm. We have referred to the Keysight manual [35] for the slim probe on the validity assumptions of the measurement. In the keysight manual, it is well documented that a minimum of 5 mm around the tip of the probe is sufficient. However, we find justification for these concepts in this literature [52].

Table 4 shows the relationship between the constant difference of the clustered curves and burn variations. The constant difference of the clustered curves is along the y-axis which is the average of average real permittivity values of the samples. It was found from this analysis that the deeper the injury (higher degree burn), the real permittivity differences of the clusters will increase. Also, it will depend on the thickness of the skin. The thickness of the samples between the layers is measured using the vernier caliper. The analysis varies based on the number of sectors in the clusters. Based on our analysis we can observe in Table 4 that full-thickness burn will have a larger real permittivity difference between 19 to 22. The deep dermal burn will have a medium real permittivity difference between 7 to 13. At last, partial thickness to deep dermal burn will have a real permittivity difference of less than 7.

In this comparison, we can clearly notice the substantial difference in the real permittivity values between healthy and burnt tissues. The dielectric profile of sectors corresponding to superficial, dermal, deep dermal, and full-thickness burns

were found to be lower values when compared to healthy sectors. Deeper injuries having lower dielectric profile values were found similar to bone and fat. This result proves the possibility of the detection of the burn degree and depths by their respective dielectric profiles. Visual-based microwave real permittivity mapping is supported by the proposed statistical analysis.

B. UNCERTAINTY IN VALUES

As part of the validation procedure, the dielectric properties of a known reference, deionized water, open air, and a short are measured to ensure the accuracy of the measurements on the skin with different properties. Keysight Technologies dielectric slim probe setup computes the uncertainty of the material (skin) parameters for transmission line and free space method. The FieldFox (VNA) measures the reflection coefficient of the skin, not its real permittivity. Materials Measurement Software model converts the reflection coefficients to real permittivity. The question of measurement uncertainty is what effect does the measured reflection co-efficient measurement error has on the converted real permittivity values. Sensitivity values can show a relative, qualitative warning of uncertainty. For example, if the first sensitivity number is 60 and the second sensitivity number is 30 and measurement uncertainties of the first sensitivity values are two times (60/30=2) those of the second sensitivity. Additionally, error sources can be in two categories: fieldfox (VNA) error sources and dielectric error sources. Examples of dielectric error sources are the slim probe model accuracy which varies 5 to 10 percent and uncertainty due to accuracy of the dielectric characterization of calibration or reference standards. We did not use the short standard from the keysight technologies; instead, we used a silver conducting sheet. The effect of the VNA error sources can be as shown in the Equation 4

$$\Delta\epsilon = N \times S \tag{4}$$

where, $\Delta\epsilon$ is the error, N is VNA uncertainty (in linear function), and S is the sensitivity number (absolute values). For instance, skin is measured $\epsilon_r = 38$ is measured at 2.45 GHz with a water/short/air calibration. At 2.45 GHz the slim probe directivity contribution would vary between 0.1 to 0.2 and the sensitivity is 20 then error = $0.2 \times 20 = 4$. Furthermore, this value is not a total measurement error, it is just a portion due to slim probe directivity. The effect of dielectric error sources can be shown in the Equation 5

$$\Delta\epsilon = \frac{SM}{SS} \times \Delta_S \tag{5}$$

where, SM and SS are the sensitivity of measured material and that of calibration standard, and Δ_S is delta uncertainty of the material used in calibration.

There are other few uncertainties in the measured values that may happen because of the following reason:

- We have not used the short standard device from Keysight Technologies for calibration [53].

- Human errors while performing the measurements for hours together.
- Thickness variation of the sample.
- Cleanliness of the slim probe tip.
- The amount of force used to press the slim probe against the skin will vary from person to person.
- Homogeneity of the region.
- Duration of air exposure during measurement.
- Variations in the burn degree of damage.

C. TARGETED APPLICATION

This work is very useful for the better design of epidermal microwave sensors for diagnostics. This work will be the extensive database for the microwave sensor design based on the real permittivity variation versus burn degree. A magnetically connected loop antenna with a spiral ring resonator was developed for this sensor to analyze burn degree. For sensing technologies, we needed a high-quality factor (Q) with a restricted band. On the Rogers RO 3003 substrate, which has a typical thickness of 0.13 mm, we developed a microwave resonator sensor with high Q. The copper trace that was arranged into a circular planar spiral served as the foundation for the design and construction of the electromagnetic resonant sensor patch. The 14-mm-radius circular spiral patch that served as the SR and loop probe had 12 turns. Our earlier work contains more details on this sensor [54]. For practical fabrication of the sensor, we have used a low-loss 12 cm long flexible cable to connect the sensor with VNA, which is suitable for up to 6 GHz experiments. On measurement time, we have done single full port calibration. In this calibration, we used the port extension option in our network analyzer to avoid cable loss. So there was no strong effect on performance of proposed sensor. This work provides the technical information needed for sensor development that is optimized for burn degree. A variety of noninvasive imaging techniques have been investigated and thoroughly reviewed in order to determine the severity of a burn [55], [56], [57], [58], [59]. The most effective application of these technologies makes use of a laser doppler imaging (LDI) technique. However, the LDI technique is having lengthy acquisition periods and high costs, we still need to make improvements before using it to identify burn wounds.

1) VALIDATING TOOL USING NON-INVASIVE MICROWAVE SPIRAL RESONATOR SENSOR

One of the other promising resonant probe technologies is the microwave-based sensor [60]. It is preferred because it is non-invasive, very sensitive, small in size, and has minimal fabrication and measurement costs [61]. The microwave sensor having a good impedance match to the body tissues, and having a narrow bandwidth to discern shifts in resonance frequency when placed above the areas of interest are essential sensor features that must be taken into account during the design of the microwave sensor. The computer simulation technology (CST Studio, 2020) simulation and optimization of the microwave senseburn sensor [54]. Figure 9 shows

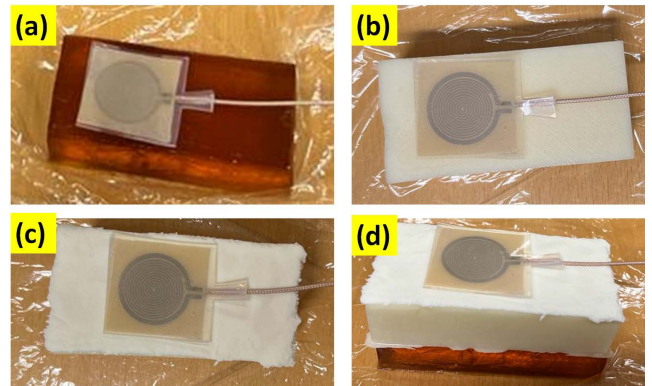


FIGURE 9. Senseburn Sensor [54] on the (a) burn tissue with edema, (b) full-thickness burn, (c) Superficial burn, and (d) Partial to deep dermal.

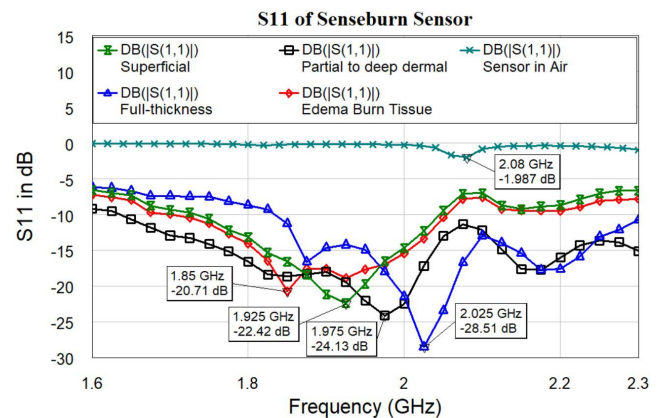


FIGURE 10. S11 measurements using senseburn sensor [54] on the burn tissue with edema, full-thickness burn, Superficial burn, Partial to deep dermal, and in Air.

that senseburn sensor is validated on the phantoms representing (a) burn tissue with edema, (b) full-thickness burn, (c) Superficial burn, and (d) Partial to deep dermal. The sensor is non-invasive and only makes superficial contact with the skin’s surface. As a result of the frequency domain analysis, the sensor should have a better match for skin contact compared to free space. The burn tissue with edema and full-thickness burn phantoms are prepared for the dimension 3 cm × 5 cm × 10 cm. Furthermore, the Superficial Burn Phantom is prepared for the dimension 2 mm × 5 cm × 10 cm. The dielectric real permittivity of the (a) burn tissue with edema, (b) full-thickness burn, (c) Superficial burn, and (d) Partial to deep dermal was found to be 56.2, 6.4, and 38.4 at 2.45 GHz. The partial to deep dermal phantoms which means Superficial Burn phantom, were placed above the full-thickness burn phantom and both were placed on the burn tissue with edema phantom. The sensor performance is based on the effective real permittivity of all three layers phantoms which represents partial to deep dermal.

Figure 10 shows the S11 measurements using the senseburn sensor on the phantom shown in Figures 9 (a)-(d). Also, illustrates the differences in resonance frequency for various dielectric constants with respect to various phantom layers.

We can observe that resonance frequency changes between 1.85 GHz to 2.025 GHz and the sensor's resonance frequency varies linearly with respect to the change in real permittivity of the material. So, this sensor can be used to assess the various burn degrees based on the resonance frequency shifts. Especially, if the sensor which detects the real permittivity variation in the reported values can be compared with results and design an efficient sensor to detect actual burnt degree. This can be an extensive database for the microwave sensor designers related to the skin to detect various burn conditions. The relationship between real permittivity and various burn conditions for microwave frequencies is explained technically in this study.

IV. CONCLUSION

The results presented in this work show a clear difference in burn variations with respect to real permittivity. We found the extent real permittivity changes for the partial thickness, deep dermal, and full-thickness burns. We have observed that deeper the burn (higher degree) will have more difference of real permittivity between healthy and burnt tissues. Overall data analysis has got the potential application in designing microwave sensors to detect the real permittivity variations on the human skin to evaluate burn degree. Also, it opens the possible way for the microwave designers to develop the sensor for skin-related disorders. In addition, using the dielectric database compiled from ex-vivo burnt human tissue samples, we created a proof-of-concept non-invasive flexible microwave sensor. This allowed us to identify phantoms with varying dielectric properties in the range of burned human tissue. We show in this paper that dielectric measurements at microwave frequencies can be used to determine the burn depth of tissue.

V. DATA AVAILABILITY

The raw datasets used and/or analysed during the current study available from the corresponding author on reasonable request.

ACKNOWLEDGMENT

The authors would like to give special thanks to Javad Ebrahimzadeh, Ph.D. Student, Waves: Core Research and Engineering (WaveCore), Leuven (Arenberg), KU Leuven for his programming work in permittivity-based microwave profiling. (*Mokhtar Kouki and Yasmina Dhouibi contributed equally to this work.*)

REFERENCES

- [1] World Health Organization. (2008). *A WHO Report Plan for Burn Prevention and Care*. [Online]. Available: <https://www.who.int/news-room/factsheets/detail/burns/>
- [2] K. Asselin. (2020). *National Burn Awareness Week 2020—American Burn Association*. [Online]. Available: <http://ameriburn.org/national-burn-awareness-week-2020/>
- [3] H. Cleland, I. Sriubaite, and B. Gabbe, "Burden and costs of severe burn injury in Victoria, Australia," *Eur. Burn J.*, vol. 3, no. 3, pp. 391–400, Jul. 2022.
- [4] Canadian Skin Patient Alliance. *CSPA—Burns*. [Online]. Available: <https://www.canadianskin.ca/burns#fast-facts>
- [5] N. Brusselaers, S. Monstrey, D. Vogelaers, E. Hoste, and S. Blot, "Severe burn injury in Europe: A systematic review of the incidence, etiology, morbidity, and mortality," *Crit. Care*, vol. 14, no. 5, pp. 1–12, 2010.
- [6] R. Papini, "Management of burn injuries of various depths," *BMJ*, vol. 329, no. 7458, pp. 158–160, Jul. 2004. [Online]. Available: <https://www.bmj.com/content/329/7458/158>
- [7] S. Rex, "Burn injuries," *Current Opinion Crit. Care*, vol. 18, no. 6, pp. 671–676, 2012.
- [8] J. M. Still, E. J. Law, K. G. Klavuhn, T. C. Island, and J. Z. Holtz, "Diagnosis of burn depth using laser-induced indocyanine green fluorescence: A preliminary clinical trial," *Burns*, vol. 27, no. 4, pp. 364–371, Jun. 2001.
- [9] H. Ye and S. De, "Thermal injury of skin and subcutaneous tissues: A review of experimental approaches and numerical models," *Burns*, vol. 43, no. 5, pp. 909–932, Aug. 2017.
- [10] T. Schulz, J. Marotz, S. Seider, S. Langer, S. Leuschner, and F. Siemers, "Burn depth assessment using hyperspectral imaging in a prospective single center study," *Burns*, vol. 48, no. 5, pp. 1112–1119, Aug. 2022.
- [11] *DATA SHEET IO Libraries Suite 2020*, Keysight Technol., Santa Rosa, CA, USA, 2020. [Online]. Available: <https://www.keysight.com/>
- [12] C. Poon, U. Sunar, D. J. Rohrbach, S. Krishnamurthy, T. Olsen, M. Kent, N. M. Weir, R. Simman, and J. B. Travers, "Early assessment of burn severity in human tissue ex vivo with multi-wavelength spatial frequency domain imaging," *Toxicol. Vitro*, vol. 52, pp. 251–254, Oct. 2018.
- [13] M. Giretzlehner, I. Ganitzer, and H. Haller, "Technical and medical aspects of burn size assessment and documentation," *Medicina*, vol. 57, no. 3, p. 242, Mar. 2021.
- [14] M. Bezuhly and J. S. Fish, "Acute burn care," *Plastic Reconstructive Surg.*, vol. 130, no. 2, pp. 349e–358e, 2012.
- [15] S. R. M. Shah, J. Velander, M. D. Perez, L. Joseph, V. Mattsson, N. B. Asan, F. Huss, and R. Augustine, "Improved sensor for non-invasive assessment of burn injury depth using microwave reflectometry," in *Proc. 13th Eur. Conf. Antennas Propag. (EuCAP)*, 2019, pp. 1–5.
- [16] J. E. Thatcher, J. J. Squiers, S. C. Kanick, D. R. King, Y. Lu, Y. Wang, R. Mohan, E. W. Selke, and J. M. DiMaio, "Imaging techniques for clinical burn assessment with a focus on multispectral imaging," *Adv. Wound Care*, vol. 5, no. 8, pp. 360–378, Aug. 2016.
- [17] T. S. England and N. A. Sharples, "Dielectric properties of the human body in the microwave region of the spectrum," *Nature*, vol. 163, no. 4143, pp. 487–488, Mar. 1949. [Online]. Available: <https://www.nature.com/articles/163487b0>
- [18] H. F. Cook, "The dielectric behaviour of some types of human tissues at microwave frequencies," *Brit. J. Appl. Phys.*, vol. 2, no. 10, p. 295, 1951.
- [19] H. P. Schwan, "Electrical properties of tissue and cell suspensions," *Adv. Biol. Med. Phys.*, vol. 5, pp. 147–209, Jan. 1957.
- [20] E. C. Burdette, P. G. Friederich, R. L. Seaman, and L. E. Larsen, "In situ permittivity of canine brain: Regional variations and postmortem changes," *IEEE Trans. Microw. Theory Techn.*, vol. MTT-34, no. 1, pp. 38–50, Jan. 1986.
- [21] H. P. Schwan and K. R. Foster, "RF-field interactions with biological systems: Electrical properties and biophysical mechanisms," *Proc. IEEE*, vol. 68, no. 1, pp. 104–113, Jan. 1980.
- [22] M. A. Stuchly, T. W. Athey, G. M. Samaras, and G. E. Taylor, "Measurement of radio frequency permittivity of biological tissues with an open-ended coaxial line: Part II—Experimental results," *IEEE Trans. Microw. Theory Techn.*, vol. MTT-30, no. 1, pp. 87–92, Jan. 1982.
- [23] R. Pethig, "Dielectric properties of biological materials: Biophysical and medical applications," *IEEE Trans. Electr. Insul.*, vol. EI-19, no. 5, pp. 453–474, Oct. 1984.
- [24] E. Alanen, T. Lahtinen, and J. Nuutinen, "Variational formulation of open-ended coaxial line in contact with layered biological medium," *IEEE Trans. Biomed. Eng.*, vol. 45, no. 10, pp. 1241–1248, Oct. 1998.
- [25] M. Zhadobov, R. Augustine, R. Sauleau, S. Alekseev, A. Di Paola, C. L. Quément, Y. S. Mahamoud, and Y. Le Dréan, "Complex permittivity of representative biological solutions in the 2–67 GHz range," *Bioelectromagnetics*, vol. 33, no. 4, pp. 346–355, May 2012.
- [26] S. Di Meo, P. F. Espin-Lopez, A. Martellosio, M. Pasian, M. Bozzi, L. Peregrini, A. Mazzanti, F. Svelto, P. E. Summers, G. Renne, L. Preda, and M. Bellomi, "Experimental validation of the dielectric permittivity of breast cancer tissues up to 50 GHz," in *IEEE MTT-S Int. Microw. Symp. Dig.*, Sep. 2017, pp. 1–3.

- [27] A. R. M. D. Perez, J. Ebrahimizadeh, K. B. Pramod, S. R. M. Shah, I. K. M. El-Ali, and F. Huss, "Dielectric profiles at microwave frequencies of different burn depths: Preliminary data from ex-vivo human (burnt) skin samples," *Eur. J. Burn Care Vuola J.*, 2019.
- [28] A. Papp, T. Lahtinen, M. Härmä, J. Nuutinen, A. Uusaro, and E. Alhava, "Dielectric measurement in experimental burns: A new tool for burn depth determination?" *Plastic Reconstruct. Surg.*, vol. 117, no. 3, pp. 889–898, Mar. 2006.
- [29] P. K. B. Rangaiah, J. Ebrahimizadeh, A. H. Nagaraju, I. El-Ali, M. Kouki, B. Mandal, F. Huss, M. D. Perez, and R. Augustine, "Clustering of dielectric and colour profiles of an ex-vivo burnt human skin sample," in *Proc. 14th Eur. Conf. Antennas Propag. (EuCAP)*, Mar. 2020, pp. 1–5.
- [30] T. K. Kataria, M. E. Sosa-Morales, J. L. Olvera-Cervantes, R. Rojas-Laguna, and A. Corona-Chavez, "Dielectric properties of pulque at different temperatures from 0.1 to 25 GHz," *J. Microw. Power Electromagn. Energy*, vol. 53, no. 4, pp. 215–224, Oct. 2019.
- [31] P. S. Mun, H. N. Ting, Y. B. Chong, and T. A. Ong, "Dielectric properties of glycosuria at 0.2–50 GHz using microwave spectroscopy," *J. Electromagn. Waves Appl.*, vol. 29, no. 17, pp. 2278–2292, Nov. 2015.
- [32] H. H. Bock, "On some significance tests in cluster analysis," *J. Classification*, vol. 2, no. 1, pp. 77–108, Dec. 1985.
- [33] M. Kozak, "'A dendrite method for cluster analysis' by Caliński and Harabasz: A classical work that is far too often incorrectly cited," *Commun. Statist., Theory Methods*, vol. 41, no. 12, pp. 2279–2280, Jun. 2012.
- [34] J. A. Hartigan, "Statistical theory in clustering," *J. Classification*, vol. 2, no. 1, pp. 63–76, Dec. 1985.
- [35] Keysight 85070E Dielectric Probe Kit 200 MHz to 50 GHz, Keysight Technol., Santa Rosa, CA, USA, 2014. [Online]. Available: <https://literature.cdn.keysight.com/litweb/pdf/5989-0222EN.pdf?id=364444>
- [36] E. Burdette, F. Cain, and J. Seals, "In vivo probe measurement technique for determining dielectric properties at VHF through microwave frequencies," *IEEE Trans. Microw. Theory Techn.*, vol. MTT-28, no. 4, pp. 414–427, Apr. 1980.
- [37] A. Peyman, C. Gabriel, E. Grant, G. Vermeeren, and L. Martens, "Variation of the dielectric properties of tissues with age: The effect on the values of SAR in children when exposed to walkie-talkie devices," *Phys. Med. Biol.*, vol. 55, no. 17, p. 5249, 2010.
- [38] P. Nopp, E. Rapp, H. Pftzner, H. Nakesch, and C. Rusham, "Dielectric properties of lung tissue as a function of air content," *Phys. Med. Biol.*, vol. 38, no. 6, p. 699, 1993.
- [39] H. Schwan and K. Li, "Capacity and conductivity of body tissues at ultra-high frequencies," *Proc. IRE*, vol. 41, no. 12, pp. 1735–1740, Dec. 1953.
- [40] P. R. Stauffer, F. Rossetto, M. Prakash, D. G. Neuman, and T. Lee, "Phantom and animal tissues for modelling the electrical properties of human liver," *Int. J. Hyperthermia*, vol. 19, no. 1, pp. 89–101, 2003.
- [41] M. Lazebnik, M. C. Converse, J. H. Booske, and S. C. Hagness, "Ultrawideband temperature-dependent dielectric properties of animal liver tissue in the microwave frequency range," *Phys. Med. Biol.*, vol. 51, no. 7, p. 1941, Mar. 2006.
- [42] C. Gabriel, D. Andreuccetti, R. Fossi, and C. Petrucci, "Parametric model for the calculation of the dielectric properties of body tissues," Nello Carrara, IFAC-CNR, Florence, Italy, Tech. Rep., 2012. [Online]. Available: <http://niremf.ifac.cnr.it>
- [43] J. J. Teres and N. York, "NESUG 2011 life in the FASTCLUS: A data-driven approach to classifying time intervals NESUG 2011 coders' corner," *Tech. Rep.*, 2011, pp. 1–4.
- [44] *The FASTCLUS Procedure, SAS/STAT 9.2 User Guide*, SAS Inst., Cary, NC, USA, 2008, pp. 1621–1674.
- [45] R. D. Andreuccetti and C. Petrucci, "An internet resource for the calculation of the dielectric properties of body tissues in the frequency range 10 Hz–100 GHz," IFAC-CNR, Florence, Italy, Tech. Rep., 1997.
- [46] B. A. Gloy and J. T. Akridge, "Segmenting the commercial producer marketplace for agricultural inputs," *Int. Food Agribusiness Manage. Rev.*, vol. 2, no. 2, pp. 145–163, Jun. 1999.
- [47] E. Süli and D. F. Mayers, *An Introduction to Numerical Analysis*. Cambridge, U.K.: Cambridge Univ. Press, 2003.
- [48] T. Sasaki and H. Murao, "Efficient Gaussian elimination method for symbolic determinants and linear systems," *ACM Trans. Math. Softw.*, vol. 8, no. 3, pp. 277–289, Sep. 1982.
- [49] A. Ben-Israel, "A Cramer rule for least-norm solutions of consistent linear equations," *Linear Algebra Appl.*, vol. 43, pp. 223–226, Mar. 1982.
- [50] E. Klafszky and T. Terlaky, "The role of pivoting in proving some fundamental theorems of linear algebra," *Linear Algebra Appl.*, vol. 151, pp. 97–118, Jun. 1991.
- [51] P. M. Meaney, A. P. Gregory, J. Seppälä, and T. Lahtinen, "Open-ended coaxial dielectric probe effective penetration depth determination," *IEEE Trans. Microw. Theory Techn.*, vol. 64, no. 3, pp. 915–923, Mar. 2016.
- [52] K. You, H. Mun, L. You, J. Salleh, and Z. Abbas, "A small and slim coaxial probe for single rice grain moisture sensing," *Sensors*, vol. 13, no. 3, pp. 3652–3663, Mar. 2013. [Online]. Available: <https://www.mdpi.com/1424-8220/13/3/3652>
- [53] Keysight. (2020). *N1501A Dielectric Probe Kit*. [Online]. Available: <https://www.keysight.com/en/pd-2492144-pn-N1501A/dielectric-probe-kit?cc=US&lc=eng>
- [54] P. K. B. Rangaiah, B. Mandal, E. Avetisyan, A. S. Chezhian, B. Augustine, M. D. Perez, and R. Augustine, "Preliminary analysis of burn degree using non-invasive microwave spiral resonator sensor for clinical applications," *Frontiers Med. Technol.*, vol. 4, Apr. 2022, Art. no. 859498. [Online]. Available: <https://www.frontiersin.org/article/10.3389/fmedt.2022.859498>
- [55] S. Kunjachan, J. Ehling, G. Storm, F. Kiessling, and T. Lammers, "Non-invasive imaging of nanomedicines and nanotheranostics: Principles, progress, and prospects," *Chem. Rev.*, vol. 115, no. 19, pp. 10907–10937, Oct. 2015.
- [56] G. C. Giakos, M. Pastorino, F. Russo, S. Chowdhury, N. Shah, and W. Davros, "Noninvasive imaging for the new century," *IEEE Instrum. Meas. Mag.*, vol. 2, no. 2, pp. 32–35, Jun. 1999.
- [57] A. K. Murray, T. L. Moore, J. B. Manning, C. Taylor, C. E. M. Griffiths, and A. L. Herrick, "Noninvasive imaging techniques in the assessment of scleroderma spectrum disorders," *Arthritis Rheumatism*, vol. 61, no. 8, pp. 1103–1111, Aug. 2009.
- [58] R. S. Balaban and V. A. Hampshire, "Challenges in small animal noninvasive imaging," *ILAR J.*, vol. 42, no. 3, pp. 248–262, Jan. 2001.
- [59] P. Schoenhagen, S. S. Halliburton, A. E. Stillman, S. A. Kuzmiak, S. E. Nissen, E. M. Tuzcu, and R. D. White, "Noninvasive imaging of coronary arteries: Current and future role of multi-detector row CT," *Radiology*, vol. 232, no. 1, pp. 7–17, Jul. 2004.
- [60] V. Mattsson, L. L. G. C. Ackermans, B. Mandal, M. D. Perez, M. A. M. Vesseur, P. Meaney, J. A. Ten Bosch, T. J. Blokhuis, and R. Augustine, "MAS: Standalone microwave resonator to assess muscle quality," *Sensors*, vol. 21, no. 16, p. 5485, Aug. 2021. [Online]. Available: <https://www.mdpi.com/1424-8220/21/16/5485>
- [61] P. K. B. Rangaiah and H. V. Kumaraswamy, "A 1–5 GHz, hybrid mic wide-band LNA utilizing microstrip geometric structure variety for performance improvement," *Trans. Netw. Commun.*, vol. 5, no. 2, p. 15, Apr. 2017.



PRAMOD K. B. RANGAIAH (Member, IEEE) was born in Mysore, Karnataka, India, in 1989. He received the B.E. degree in electronics and communication from the Dr. Ambedkar Institute of Technology, Visvesvaraya Technological University, Belagavi, in 2010, and the M.Tech. degree in RF communication and the Ph.D. degree in electronics engineering from Jain University, Bengaluru, in 2012. He worked as an RF Design Trainee at Icon Design and Automation Private

Ltd., and a Visiting Research Scholar at the University of Concordia, Montreal, QC, Canada. He is currently working as a Researcher with the Division of Solid-State Electronics, Microwaves in Medical Engineering Group, Department of Electrical Engineering Sciences, Ångström Laboratory, Uppsala University, Sweden. His research interests include design, characterization, optimization of RF passive devices, board level tuning, optimization of matching networks, low-noise amplifier, power amplifier, circuit linearization, high-efficiency design techniques, and circuit instability and strategies. He is a member of ISTE and a Life Member of IETE. He is an Associate Editor of the *International Journal of Big Data Management* (Inderscience Publishers) and an Editorial Board Member of *Frontiers and International Journal of Advanced And Applied Sciences*. He is also a regular peer reviewer for various prestigious international journals, such as IEEE ACCESS, MDPI, Inderscience Publishers, *Advances in Science, Technology and Engineering Systems Journal*, and *International Journal of Advance Research and Innovative Ideas in Education*.

MOKHTAR KOUKI, photograph and biography not available at the time of publication.

YASMINA DHOUBI, photograph and biography not available at the time of publication.

FREDRIK HUSS, photograph and biography not available at the time of publication.



BAPPADITYA MANDAL (Member, IEEE) was born in India, in 1985. He received the B.Tech. degree in electronics and communication engineering from the Kalyani Government Engineering College, Maulana Abul Kalam Azad University of Technology (Formerly WBUT), West Bengal, in 2008, and the M.E. degree in advanced communication and networking and the Ph.D. degree in microwave and antenna engineering from the Indian Institute of Engineering Science and Technology (IEST), Shibpur, India, in 2010 and 2018, respectively.

He is currently working as a Researcher with the Division of Solid-State Electronics, Microwaves in Medical Engineering Group (MMG), Department of Electrical Engineering, Ångström Laboratory, Uppsala University (UU), Sweden. His current research interests include wearable antennas implantable antenna and non-invasive microwave sensors for biomedical applications. He has served as a Regular Reviewer for various prestigious SCI journals, such as *IET Electronics Letters*, *IEEE TRANSACTIONS ON ANTENNAS AND PROPAGATION*, and *RFCAD*.



BOBINS AUGUSTINE received the B.Sc. degree in physics from Mahatma Gandhi University, Kottayam, India, in 2008, the master's degree in applied physics from the Cochin University of Science and Technology (CUSAT), India, in 2010, and the D.Sc.Tech. degree from the University of Oulu, Finland, in 2016. After working as a Project Fellow at CUSAT, he received Nordic Scholarship to do his doctorate in printed electronics at the University of Oulu, in 2011. Since then, he has

been working as a Postdoctoral Researcher and a Specialist in the field of printed electronics. Since 2019, he has been a Visiting Researcher with Linköping University, Sweden. He is currently working as a Researcher with Uppsala University, Sweden, and the Uppsala Networked Objects (UNO)/Department of Information Technology and the Microwaves in Medical Engineering Group (MMG)/Department of Electrical Engineering. He was also a part of many renowned Finnish projects funded by HILLA and Business Finland (Tekes). His research interests include flexible printed electronic devices, such as sensors, antennas, OLEDs, solar cells, OTFTs, conducting polymers/transparent conducting oxides, and soft robotics and actuators. In the beginning of 2021, he won the prestigious and highly competitive Marie Skłodowska Curie Fellowship-H2020 IF from EU Research Executive Agency for his project proposal titled Soft Amphibious Micro Robots fabricated by Additive Integrated manufacturing (SAMURAI) and it is intended for in-vivo micro robotic surgery and drug delivery.



MAURICIO DAVID PEREZ (Member, IEEE) was born in Buenos Aires, Argentina, in 1980. He received the Engineering degree in electronics from the National Technological University (UTN), Argentina, in 2007, and the Ph.D. degree in electrical engineering from the University of Bologna (UNIBO), Italy, in 2012. From 2012 to 2014, he was an Industrial Researcher in Italy. From 2014 to 2017, he was an Academic Teacher and a Researcher with UTN.

He is currently a Teacher and a Researcher with the Ångström Laboratories, Microwaves in Medical Engineering Group (MMG), Uppsala University (UU), Sweden. His current research interest includes modeling and data-driven validation of microwave sensors for biomedical applications.



ROBIN AUGUSTINE (Member, IEEE) received the degree in electronics science from Mahatma Gandhi University, India, in 2003, the master's degree in electronics with robotics specialization from the Cochin University of Science and Technology, India, in 2005, and the Ph.D. degree in electronics and optic systems from the Université Paris-Est Marne-La-Vallée, France, in July 2009. He was a Postdoctoral Researcher at the University of Rennes 1, Brittany, France, from 2009 to 2011.

He joined Uppsala University as a Senior Researcher, in 2011. He became an Associate Professor with Uppsala University, in February 2016. He is currently a Senior University Lecturer in medical engineering and a Docent in microwave technology. He is also the Head of the Microwaves in Medical Engineering Group (MMG), and the Founder, the Chairperson, and the CTO of Probingon AB, Swedish Medtech Company. He was a part of Vinnova Project on skin cancer diagnostic tool based on micromachined interface for high-resolution THz spectroscopy (MTSSC). He is a Co-PI of the EU Project SINTEC, SSF framework grant LifeSec, Vinnova grant connect my body, in 2018, and the SSF framework grant Zero-IoT 2020, the Research Lead of the Eurostars Project SenseBurn 2018, and the Project Leader of Eurostars Project MAS 2020. He is also an EU Coordinator of HORIZON 2020 FET-OPEN Science Excellence Project B-CRATOS, a visionary project in man machine interface. He has been invited at the Swedish Royal Academy of Sciences to present his work on noninvasive physiological sensing. He is also a Project Coordinator for Indo-Swedish Vinnova Project BDAS and Swedish part of the bilateral (The Netherlands and Sweden) Horizon 2020 Eurostars Project COMFORT. He is the author or coauthor of more than 180 publications, including journals and conferences and has three patents. His thesis topic was "Electromagnetic modeling of human tissues and its application on the interaction between antenna and human body in the BAN context." Two Ph.D. students graduated in 2019 under his supervision. He has received Carl Trygger and Olle Engqvist fundings for his postdoctoral research. His current research interests include designing of wearable antennas, BMD sensors, microwave phantoms, dielectric characterization, bionics, mechatronics, non-invasive diagnostics, point of care sensors for physiological monitoring, clinical trials, animal trials, and on body microwave communication. He has pioneered the Fat—Intra Body Communication Technique. He was a recipient of UGCRFSMS fellowship from Indian Government and EGIDE Eiffel grant for excellence from French Research Ministry, in 2006 and 2008, respectively, and the Swedish Research Agency, Vetenskapsrådet's (VR) Project grant 2017 for his project on "A Novel Modality for Osteodiagnosis" and the Attractive Innovation Project 2020 Award from Uppsala University Innovation. He is the Regular Sessions Chair and a Convened Session Organizer of EuCAP. He is an Editorial Board Member of *IET Electronics Letters* and *Frontiers in Communication*. He has been a Board Member with the Department of Electrical Engineering, since January 2020.

...